



Article

Thioredoxin Reductase-Type Ferredoxin: NADP⁺ Oxidoreductase of *Rhodopseudomonas palustris*: Potentiometric Characteristics and Reactions with Nonphysiological Oxidants

Mindaugas Lesanavičius ¹, Daisuke Seo ² and Narimantas Čėnas ^{1,*}

¹ Department of Xenobiotics Biochemistry, Institute of Biochemistry of Vilnius University, Saulėtekio 7, LT-10257 Vilnius, Lithuania; mindaugas.lesanavicius@gmc.vu.lt

² Division of Material Sciences, Graduate School of Natural Science and Technology, Kanazawa University, Kakuma, Kanazawa 920-1192, Japan; dseo@se.kanazawa-u.ac.jp

* Correspondence: narimantas.cenas@bchi.vu.lt

Abstract: *Rhodopseudomonas palustris* ferredoxin:NADP⁺ oxidoreductase (*RpFNR*) belongs to a novel group of thioredoxin reductase-type FNRs with partly characterized redox properties. Based on the reactions of *RpFNR* with the 3-acetylpyridine adenine dinucleotide phosphate redox couple, we estimated the two-electron reduction midpoint potential of the FAD cofactor to be -0.285 V. 5-Deaza-FMN-sensitized photoreduction revealed -0.017 V separation of the redox potentials between the first and second electron transfer events. We examined the mechanism of oxidation of *RpFNR* by several different groups of nonphysiological electron acceptors. The $k_{\text{cat}}/K_{\text{m}}$ values of quinones and aromatic *N*-oxides toward *RpFNR* increase with their single-electron reduction midpoint potential. The lower reactivity, mirroring their lower electron self-exchange rate, is also seen to have a similar trend for nitroaromatic compounds. A mixed single- and two-electron reduction was characteristic of quinones, with single-electron reduction accounting for 54% of the electron flux, whereas nitroaromatics were reduced exclusively via single-electron reduction. It is highly possible that the FADH \cdot to FAD oxidation reaction is the rate-limiting step during the reoxidation of reduced FAD. The calculated electron transfer distances in the reaction with quinones and nitroaromatics were close to those of *Anabaena* and *Plasmodium falciparum* FNRs, thus demonstrating their similar “intrinsic” reactivity.

Keywords: *Rhodopseudomonas palustris*; ferredoxin:NADP⁺ oxidoreductase; thioredoxin reductase; quinones; nitroaromatic compounds; reduction mechanism; redox potential



Citation: Lesanavičius, M.; Seo, D.; Čėnas, N. Thioredoxin Reductase-Type Ferredoxin: NADP⁺ Oxidoreductase of *Rhodopseudomonas palustris*: Potentiometric Characteristics and Reactions with Nonphysiological Oxidants. *Antioxidants* **2022**, *11*, 1000. <https://doi.org/10.3390/antiox11051000>

Academic Editor: Stanley Omaye

Received: 25 April 2022

Accepted: 17 May 2022

Published: 19 May 2022

Publisher's Note: MDPI stays neutral with regard to jurisdictional claims in published maps and institutional affiliations.



Copyright: © 2022 by the authors. Licensee MDPI, Basel, Switzerland. This article is an open access article distributed under the terms and conditions of the Creative Commons Attribution (CC BY) license (<https://creativecommons.org/licenses/by/4.0/>).

1. Introduction

Ferredoxin:NADP⁺ oxidoreductases (FNRs) transfer redox equivalents between NADP(H) and the low-redox-potential FeS protein ferredoxin (Fd), or flavodoxin, a low-molecular-weight flavin mononucleotide (FMN)-containing protein [1–7]. FNRs comprise separate flavin adenine dinucleotide (FAD)- and NADP(H)-binding domains. The stabilization of the neutral (blue) FAD semiquinone (FADH \cdot) as the reaction intermediate takes place by transforming the two-electron (hydride) transfer into two single-electron transfer events [1,2,8]. The complex formation between FNR and Fd is frequently attributed to the electrostatic and hydrophobic interactions [2,6,9].

FNRs are found in a wide variety of organisms and are classified into several groups and subclasses, whose representatives differ in amino acid sequence, catalytic rate, specificity for NAD(P)(H), physiological functions, and direction of electron transfer [3,7,10]. Most recently, a distinctive subclass of thioredoxin reductase-type FNRs has been discovered, whose structure exhibits the low M_r thioredoxin reductase (TrxR) fold ([10], and references therein). This fold consists of two domains with Rossmann-like three-layer $\beta\beta\alpha$ sandwich folds that bind FAD and NADP(H). The typical representatives of this subclass

are dimeric FNRs of the green sulfur bacterium *Chlorobaculum tepidum* [11,12], the heterotrophic Gram-positive bacterium *Bacillus subtilis* [13–15], and the photosynthetic purple nonsulfur bacterium *Rhodospseudomonas palustris* [15,16]. In these enzymes, the residues of the NADP(H)-binding domain are inserted between the two sections of the FAD-binding domain residues, and a hinge region connects the two domains (Figure 1). The rotation of the domains relative to each other may take place in catalysis, e.g., in *B. subtilis* FNR, NADP⁺ is bound ca. 15 Å away from the isoalloxazine ring of FAD, which is too distant for efficient hydride transfer [13]. The redox properties of Trx-type FNRs have been characterized partly, limited mostly by the studies of their reactions with NADP⁺/NADPH and Fds.

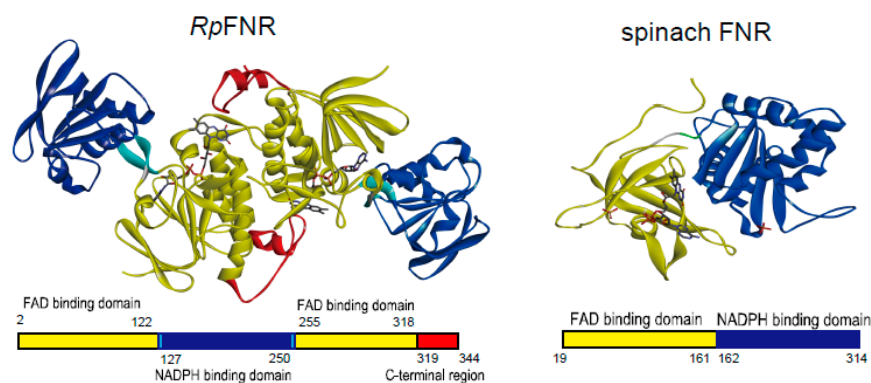


Figure 1. Ribbon diagrams of *RpFNR* (homo-dimer, PDB ID: 5YGQ) and spinach FNR (PDB ID: 1FNB). The domain organizations are indicated at the bottom. FAD-binding and NADP⁺/H-binding domains are colored yellow and blue, respectively, and the C-terminal region of *RpFNR* is in red. Bound FAD co-factor is represented as a stick model. The figure was prepared using BIOVIA Discovery Studio Visualizer (Ver. 21.1, Dassault Systèmes).

R. palustris TrxR-type FNR (RPA3954, *RpFNR*, EC 1.18.1.2) consists of the FAD-binding domain (residues 2–122 and 255–344, including the flexible C-terminal region, residues 319–344) containing a specific Tyr328 residue covering the *re* side of the isoalloxazine ring, and the NADP(H)-binding domain (residues 127–250). The reduction of *RpFNR* by NADPH and reoxidation by NADP⁺ proceeds in several phases, the fastest ones exceeding 500 s^{−1}, and involves the formation of several intermediate charge-transfer complexes [16]. On the other hand, *RpFNR* has low reactivity toward Fe₂S₂-type ferredoxin (RPA3956), whereas its reactivity toward Fe₄S₄-type Fds of *R. palustris* has not been reported [15].

In order to extend the understanding of the redox properties of *RpFNR*, we investigated its reactions with nonphysiological electron acceptors with different structures and single-electron reduction potentials (E^{17}). It is worth noting that *R. palustris* is capable of metabolizing aromatic compounds formed during plant degradation, which may involve FNR/Fd and cytochrome P-450-dependent redox systems [17,18]. Besides, some FNRs, such as the malaria parasite *Plasmodium falciparum* FNR, are a potential target for redox active drug candidates, quinones and nitroaromatic compounds [19,20]. In order to quantitatively analyze the obtained results, the redox potentials of *RpFNR* were also determined in this work.

2. Materials and Methods

2.1. Enzymes and Reagents

Recombinant *R. palustris* ferredoxin:NADP⁺ oxidoreductase was prepared as previously described [16]. Its concentration was determined spectrophotometrically according to $\epsilon_{466} = 10.8 \text{ mM}^{-1} \text{ cm}^{-1}$ [16]. 2,4,6-Trinitrotoluene (TNT) and 2,4,6-trinitrophenyl-*N*-methylnitramine (tetryl), synthesized as described [21], and 3-amino-1,2,4-benzotriazine-1,4-dioxide (tirapazamine) and its 7-methyl- and 7-fluoro- derivatives, synthesized according to [22], were a generous gift from Dr. Jonas Šarlauskas (Institute of Biochemistry,

Vilnius). 5-(1-Aziridinyl)-2,4-dinitrobenzamide (CB-1954) synthesized as described in [23], was a generous gift from Dr. Vanda Miškinienė (Institute of Biochemistry, Vilnius). The above compounds were characterized by their melting points and their $^1\text{H-NMR}$, UV, and IR spectra. The purity of compounds determined using HPLC-MS (LCMS-2020, Shimadzu, Kyoto, Japan) was >98%. NADPH, 3-acetylpyridine adenine dinucleotide phosphate (AcPyP⁺), horse heart cytochrome *c*, superoxide dismutase, and other reagents were obtained from Sigma-Aldrich (St. Louis, MO, USA) and used as received.

2.2. Photoreduction of RpFNR

RpFNR (16–17 μM) photoreduction was performed under anaerobic conditions in 0.02 M HEPES buffer, pH 7.0, using 5-deaza-FMN (0.125 μM) and EDTA (8 mM) as photosensitizers. Before protein introduction from a concentrated stock solution, the solution in a sealed spectrophotometer cuvette was flushed with O₂-free argon for 60 min. Here and in subsequent experiments, a Cary60 UV-Vis (Agilent Technologies, Santa Clara, CA, USA) or a PerkinElmer Lambda 25 UV-VIS spectrophotometer (PerkinElmer, Waltham, MA, USA) was used. Subsequently, the cell was irradiated for short periods at 20 °C with a 100 W incandescent lamp (Osram) at a distance of 20 cm; the progress of the reaction was followed spectrophotometrically for 1–1.5 h. The maximal amount of neutral semiquinone (E-FADH[•]) formed under irradiation was assumed to be defined by the inflection point of the A₆₀₀ vs. A₄₆₆ plot. The FAD semiquinone concentration was calculated using $\epsilon_{600} = 5.0 \text{ mM}^{-1}\text{cm}^{-1}$ [24]. The separation between the two single-electron-transfer potentials (ΔE^{1_7}) was further calculated from the semiquinone formation constant K_s (Equations (1) and (2)):

$$[\text{E-FADH}]_{\text{max}}/[\text{E-FAD}]_{\text{tot}} = K_s^{1/2}/(2 + K_s^{1/2}), \quad (1)$$

$$\Delta E^{1_7} = E_7(\text{E-FAD}/\text{E-FADH}) - E_7(\text{E-FADH}/\text{E-FADH}^-) = 0.059 \text{ V} \times \log K_s, \quad (2)$$

where $[\text{E-FADH}]_{\text{max}}$ is the maximal amount of formed semiquinone, $E_7(\text{E-FAD}/\text{E-FADH})$ is the potential of oxidized/semiquinone couple, $E_7(\text{E-FADH}/\text{E-FADH}^-)$ is the potential of semiquinone/reduced FAD couple, and $[\text{E-FAD}]_{\text{tot}}$ is the total enzyme concentration [25].

2.3. Steady-State Kinetic Studies

The kinetic experiments were performed spectrophotometrically in 0.02 M HEPES + 1 mM EDTA buffer (pH 7.0), at 25 °C. The kinetic data were fitted to a parabolic expression in SigmaPlot (v. 11.0, SPSS Inc., Chicago, IL, USA) to yield the steady-state parameters of the reactions, catalytic constants ($k_{\text{cat(app.)}}$), and bimolecular rate constants (k_{cat}/K_m) of the oxidants under fixed concentrations of NADPH. They are equal to the reciprocal intercepts and slopes of Lineweaver–Burk plots, $[E]/v$ vs. $1/[\text{oxidant}]$, respectively, where $[E]$ is the enzyme concentration, and v is the reaction rate. k_{cat} represents the number of molecules of NADPH oxidized by a single active center of the enzyme per second at saturated concentrations of both substrates. Kinetic parameters of steady-state reactions according to a “ping-pong” mechanism were calculated according to Equation (3):

$$\frac{v}{[E]} = \frac{k_{\text{cat}} [S][Q]}{K_{m(S)}[Q] + K_{m(Q)} [S] + [S][Q]}, \quad (3)$$

where S stands for NADPH, and Q stands for the electron acceptor. The competitive inhibition constant (K_{is}) of NADP⁺ (I) vs. NADPH was calculated according to Equation (4):

$$\frac{v}{[E]} = \frac{k_{\text{cat(app)}} [S]}{K_{m(S)} \left(1 + \frac{[I]}{K_{is}}\right) + [S]}, \quad (4)$$

and the noncompetitive inhibition constant (K_{ii}) of NADP^+ vs. electron acceptor (Q) was calculated according to Equation (5):

$$\frac{v}{[E]} = \frac{k_{\text{cat(app)}} [Q]}{(K_{\text{m(Q)}} + [Q]) \left(1 + \frac{[I]}{K_{ii}}\right)}. \quad (5)$$

The rates of enzymatic NADPH oxidation in the presence of quinones, nitroaromatic compounds, or tirapazamine derivatives were determined using the value $\Delta\epsilon_{340} = 6.2 \text{ mM}^{-1} \text{ cm}^{-1}$. The rates were corrected for the intrinsic NADPH-oxidase activity of *RpFNR*, 0.12 s^{-1} . In separate experiments, in which $50 \text{ }\mu\text{M}$ cytochrome *c* was additionally added into the reaction mixture, its quinone- or nitroaromatic-mediated reduction was assessed using the value $\Delta\epsilon_{550} = 20 \text{ mM}^{-1} \text{ cm}^{-1}$. The ferricyanide reduction rate was measured using the value $\Delta\epsilon_{420} = 1.03 \text{ mM}^{-1} \text{ cm}^{-1}$. The rate of the *RpFNR*-catalyzed reduction of AcPyP^+ by NADPH was determined using the value $\Delta\epsilon_{363} = 5.6 \text{ mM}^{-1} \text{ cm}^{-1}$ [26]. AcPyPH , the reduced form of AcPyP^+ , was prepared in situ by the reduction of AcPyP^+ with 10 mM glucose-6-phosphate and 0.01 mg/mL glucose-6-phosphate dehydrogenase. AcPyPH concentration was determined according to $\epsilon_{365} = 7.8 \text{ mM}^{-1} \text{ cm}^{-1}$ [26]. The statistical analysis was performed using Statistica (version 4.3, Statsoft, Toronto, ON, Canada).

2.4. Presteady-State Kinetic Studies

The rapid kinetic studies of *RpFNR* were performed using a SX20 stopped-flow spectrophotometer (Applied Photophysics, Leatherhead, UK) under aerobic conditions. The enzyme reduction by NADPH and its reoxidation was monitored between 450 and 800 nm , as further described in the Results section. During turnover studies, *RpFNR* in the first syringe ($4.0 \text{ }\mu\text{M}$ after mixing) was mixed with the contents of the second syringe ($50 \text{ }\mu\text{M}$ NADPH and $250 \text{ }\mu\text{M}$ tetramethyl-1,4-benzoquinone after mixing). The control experiments were performed in the absence of quinone. The reoxidation kinetics were analyzed by the method of Chance [27] according to Equation (6), where k_{ox} is the apparent first-order rate constant of enzyme reoxidation, $[\text{NADPH}]_0$ is the initial NADPH concentration, $[\text{E}_{\text{red}}]_{\text{max}}$ is the maximal concentration of the reduced enzyme formed during the turnover, and $t_{1/2(\text{off})}$ is the time interval between the formation of the half-maximal amount of E_{red} and its decay to the half-maximal value:

$$k_{\text{ox}} = [\text{NADPH}]_0 / ([\text{E}_{\text{red}}]_{\text{max}} \times t_{1/2(\text{off})}). \quad (6)$$

3. Results

3.1. Determination of Redox Potentials of *RpFNR*

According to the best of our knowledge, the potentiometric characteristics of *RpFNR* were unavailable so far. In order to determine the standard redox potential (E^0_7 , potential of E-FAD/E-FADH[−] redox couple) of *RpFNR*, we examined its reactions with the analogue of NADP(H), 3-acetylpyridine adenine dinucleotide phosphate, AcPyP(H) ($E^0_7 = -0.258 \text{ V}$). AcPyP^+ was chosen instead of NADP^+ because the reduction of NADP^+ by *RpFNR* under steady-state conditions is problematic due to the lack of a suitable electron donor [15]. During the enzymatic reduction of AcPyP^+ by NADPH, the maximum reaction rate was reached at $200 \text{ }\mu\text{M}$ NADPH. In this reaction, $k_{\text{cat}} = 53.3 \pm 3.1 \text{ s}^{-1}$, and $k_{\text{cat}}/K_{\text{m}}$ for AcPyP^+ is estimated to be $2.27 \pm 0.35 \times 10^6 \text{ M}^{-1} \text{ s}^{-1}$ (Figure 2A).

In the reverse reaction using AcPyPH generated in situ and 1.0 mM ferricyanide as an electron acceptor, $k_{\text{cat}} = 18.6 \pm 0.7 \text{ s}^{-1}$, and $k_{\text{cat}}/K_{\text{m}}$ for AcPyPH is calculated to be $6.0 \pm 0.6 \times 10^5 \text{ M}^{-1} \text{ s}^{-1}$ on the two-electron basis (Figure 2A). According to the Haldane relationship, the equilibrium constant (K) of the redox reaction with the $\text{AcPyP}^+/\text{AcPyPH}$ couple corresponds to the ratio of $k_{\text{cat}}/K_{\text{m}}$ for AcPyPH and AcPyP^+ , respectively. According to the Nernst equation, the difference between the redox potentials of the reactants, ΔE^0 , equals $0.0295 \text{ V} \times \log K$. This provides the K value of 0.264 ± 0.067 , and the E^0_7 value for the enzyme of $-0.276 \pm 0.003 \text{ V}$, respectively.

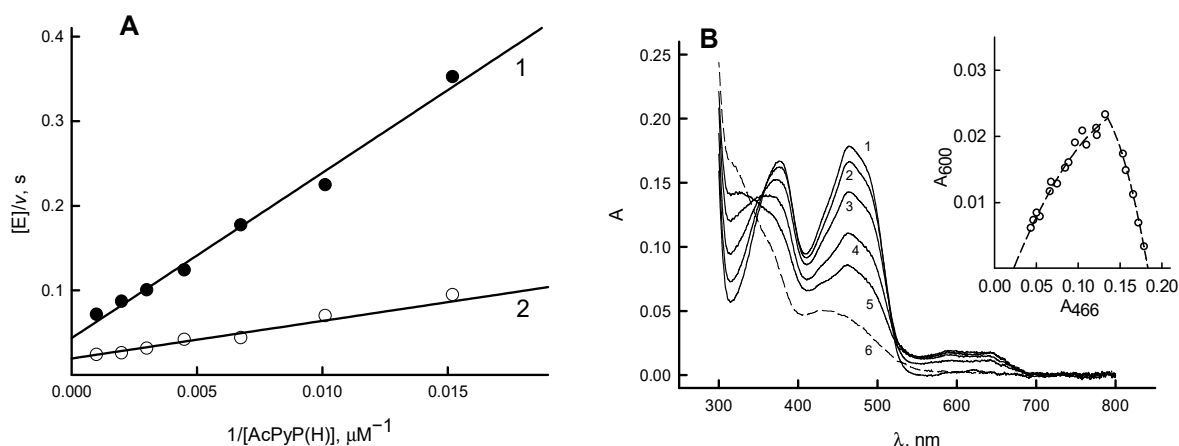


Figure 2. Determination of redox potentials of *RpFNR*. **(A)** Rates of *RpFNR*-catalyzed oxidation of AcPyPH with 1 mM ferricyanide (1), and of *RpFNR*-catalyzed reduction of AcPyP⁺ with 200 μM NADPH (2). **(B)** Spectra obtained during the photoreduction of 16.6 μM *RpFNR* at different times of illumination: immediately after mixing (1), after 10 min (2), 25 min (3), 40 min (4), 50 min (5), and after 70 min (6, fully reduced enzyme). Inset shows the interdependence of absorbance changes at 466 and 600 nm during photoreduction.

During the photoreduction of *RpFNR* in the presence of 5-deaza-FMN and EDTA, the neutral FAD semiquinone (FADH[•]) with the characteristic absorbance at 550–650 nm is formed (Figure 2B). The amount of E-FADH[•] calculated using $\epsilon_{600} = 5.0 \text{ mM}^{-1}\text{cm}^{-1}$ [24] and the data from the inset of Figure 2B is 26.5%. According to Equations (1) and (2), this gives $K_s = 0.520$, and $\Delta E^1_7 = -0.017 \text{ V}$, which corresponds to $E_7(\text{E-FAD} / \text{E-FADH}^{\bullet}) = -0.285 \text{ V}$ and $E_7(\text{E-FADH}^{\bullet} / \text{E-FADH}^{-}) = -0.268 \text{ V}$. However, a slight correction for these potentials is not ruled out, as the ϵ_{600} of FADH of *RpFNR* is not definitely determined.

3.2. Steady-State Kinetics and Oxidant Substrate Specificity Studies of *RpFNR*

The previous kinetic studies of *RpFNR* were performed using the classical nonphysiological electron acceptor of FNRs, ferricyanide [16]. We preliminarily identified a representative of another group of compounds, juglone (5-hydroxy-1,4-naphthoquinone) as an efficient nonphysiological electron acceptor of *RpFNR*. A series of parallel lines obtained in Lineweaver–Burk plots at varied concentrations of NADPH and fixed concentrations of juglone are indicative of a “ping-pong” mechanism for the quinone reductase activity of *RpFNR* (Figure 3).

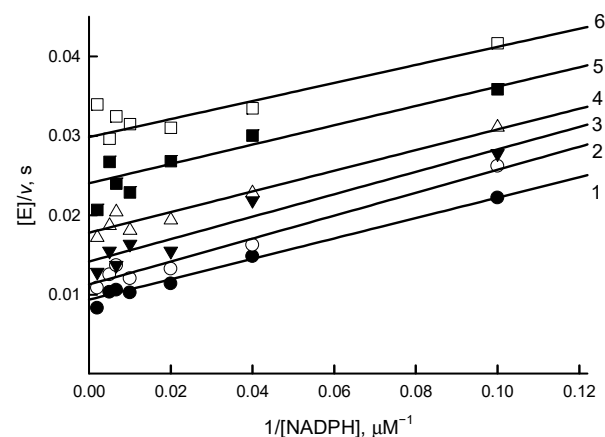


Figure 3. Lineweaver–Burk plot of the steady state kinetics of oxidation of NADPH catalyzed by *RpFNR* in the presence of juglone. Juglone concentrations are 200 μM (1), 133 μM (2), 89 μM (3), 59 μM (4), 39 μM (5), and 26 μM (6).

As deduced from Equation (3), the k_{cat} value for the juglone reduction at infinite NADPH concentration is equal to $157 \pm 7.0 \text{ s}^{-1}$, and the values of the bimolecular rate constants ($k_{\text{cat}}/K_{\text{m}}$) for NADPH and juglone are equal to $8.7 \pm 0.7 \times 10^6 \text{ M}^{-1}\text{s}^{-1}$ and $1.62 \pm 0.15 \times 10^6 \text{ M}^{-1}\text{s}^{-1}$, respectively. The value of $k_{\text{cat}}/K_{\text{m}}$ for NADPH is similar to that obtained previously, $5.5 \times 10^6 \text{ M}^{-1}\text{s}^{-1}$, using ferricyanide as the acceptor [16].

Next, we assessed the oxidant substrate specificity of *RpFNR*, examining its reactions with quinones (Q), nitroaromatic compounds (ArNO_2), and aromatic *N*-oxides ($\text{ArN} \rightarrow \text{O}$), which comprise three distinct groups of electron acceptors characterized by single-electron reduction midpoint potentials (E^{1_7}) in the range of 0.09 to -0.494 V . These compounds were studied along with several single-electron acceptors such as ferricyanide, $\text{Fe}(\text{EDTA})^-$, and benzylviologen. The studied compounds included the explosives tetryl and 2,4,6-trinitrotoluene, antibacterial agents nitrofurantoin and nifuroxime, and anticancer agents CB-1954 and tirapazamine. The apparent maximal reduction rate constants, $k_{\text{cat}(\text{app})}$, of electron acceptors at $100 \mu\text{M}$ NADPH and their respective $k_{\text{cat}}/K_{\text{m}}$ are given in Table 1.

Table 1. Steady-state rate constants of the reduction of nonphysiological electron acceptors by $100 \mu\text{M}$ NADPH catalyzed by *RpFNR*. The E^{1_7} values of compounds taken from [22,28,29].

No.	Compound	E^{1_7} (V)	$k_{\text{cat}(\text{app})}$ (s^{-1})	$k_{\text{cat}}/K_{\text{m}}$ ($\text{M}^{-1}\text{s}^{-1}$)
Quinones				
1	1,4-Benzoquinone	0.090	130 ± 16	$9.4 \pm 0.8 \times 10^5$
2	2- CH_3 -1,4-benzoquinone	0.010	130 ± 12	$5.6 \pm 0.6 \times 10^5$
3	2,6-(CH_3) ₂ -1,4-benzoquinone	-0.070	52.1 ± 1.8	$2.1 \pm 0.13 \times 10^5$
4	5-OH-1,4-naphthoquinone	-0.090	138.5 ± 9.3	$1.5 \pm 0.23 \times 10^6$
5	5,8-(OH) ₂ -1,4-naphthoquinone	-0.110	45.4 ± 3.4	$3.5 \pm 0.2 \times 10^6$
6	9,10-Phenanthrene quinone	-0.120	34.6 ± 2.4	$2.0 \pm 0.4 \times 10^6$
7	1,4-Naphthoquinone	-0.150	110 ± 13	$2.3 \pm 0.4 \times 10^5$
8	2- CH_3 -1,4-naphthoquinone	-0.200	21.6 ± 2.1	$6.0 \pm 0.8 \times 10^4$
9	(CH_3) ₄ -1,4-benzoquinone(duroquinone)	-0.260	4.07 ± 0.53	$1.1 \pm 0.1 \times 10^4$
10	9,10-Anthraquinone-2-sulphonate	-0.380	3.56 ± 0.33	$1.0 \pm 0.16 \times 10^4$
11	2-OH-1,4-naphthoquinone	-0.410	0.26 ± 0.03	$3.1 \pm 0.2 \times 10^3$
12	2- CH_3 -3-OH-1,4-naphthoquinone	-0.460	1.35 ± 0.13	$4.8 \pm 0.4 \times 10^3$
Nitroaromatic compounds				
13	Tetryl	-0.191	5.69 ± 0.14	$4.35 \pm 0.30 \times 10^4$
14	<i>N</i> -methylpicramide	-0.225	1.93 ± 0.26	$4.8 \pm 0.6 \times 10^3$
15	2,4,6-Trinitrotoluene	-0.253	1.30 ± 0.13	$2.43 \pm 0.14 \times 10^3$
16	Nifuroxime	-0.255	4.40 ± 0.32	$6.9 \pm 0.4 \times 10^3$
17	Nitrofurantoin	-0.255	2.21 ± 0.12	$5.1 \pm 0.5 \times 10^3$
18	<i>p</i> -Dinitrobenzene	-0.257	2.21 ± 0.35	$3.1 \pm 0.2 \times 10^3$
19	<i>o</i> -Dinitrobenzene	-0.287	0.48 ± 0.07	$1.28 \pm 0.2 \times 10^3$
20	4-Nitrobenzaldehyde	-0.325	0.97 ± 0.13	$2.38 \pm 0.4 \times 10^3$
21	3,5-Dinitrobenzoic acid	-0.344	0.09 ± 0.01	$2.91 \pm 0.2 \times 10^3$
22	<i>m</i> -Dinitrobenzene	-0.348	0.42 ± 0.06	$9.6 \pm 0.7 \times 10^2$
23	4-Nitroacetophenone	-0.355	0.30 ± 0.05	$8.0 \pm 0.67 \times 10^2$
24	CB-1954	-0.385	0.52 ± 0.05	$1.75 \pm 0.14 \times 10^3$
25	4-Nitrobenzyl alcohol	-0.475	0.23 ± 0.03	$2.50 \pm 0.16 \times 10^2$
Aromatic <i>N</i> -oxides				
26	7-F-tirapazamine	-0.400	1.20 ± 0.11	$1.80 \pm 0.31 \times 10^3$
27	Tirapazamine	-0.456	0.53 ± 0.04	$9.41 \pm 0.82 \times 10^2$
28	7- $\text{C}_2\text{H}_5\text{O}$ -tirapazamine	-0.494	0.46 ± 0.03	$4.91 \pm 0.32 \times 10^3$
Single-electron acceptors				
29	Ferricyanide ^a	0.410	394 ± 19	$8.8 \pm 1.0 \times 10^6$
30	$\text{Fe}(\text{EDTA})^-$	0.120	1.2 ± 0.1	$2.4 \pm 0.2 \times 10^3$
31	Benzylviologen	-0.354	19.6 ± 2.3	$3.6 \pm 0.3 \times 10^4$

^a On the single-electron basis.

The $\log k_{\text{cat}}/K_{\text{m}}$ values of nitroaromatics exhibit a linear although scattered dependence on their E^{1_7} (Table 1 and Figure 4). In general, the $\log k_{\text{cat}}/K_{\text{m}}$ values of quinones, including the single-electron acceptor benzylviologen, and $\text{ArN} \rightarrow \text{O}$, are higher than those of ArNO_2 , and demonstrate a parabolic dependence on their E^{1_7} values (Figure 4).

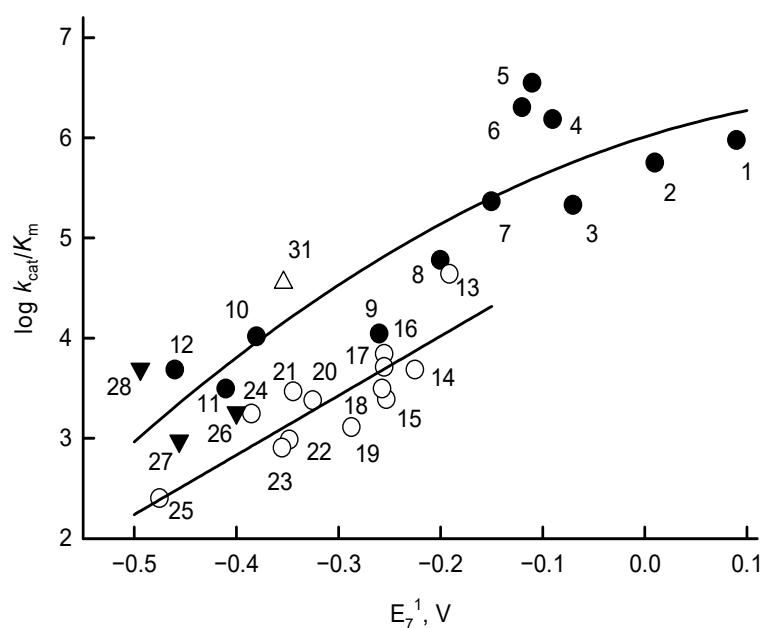


Figure 4. Dependence of the reactivity ($\log k_{\text{cat}}/K_m$) of quinones (solid circles), nitroaromatic compounds (blank circles), aromatic *N*-oxides (solid triangles), and benzylviologen (blank triangle) on their single-electron reduction midpoint potentials (E_7^1). Numbers and reduction potentials of compounds are given in Table 1.

It is established that FNRs from spinach, *Anabaena* spp. and *Plasmodium falciparum* reduce quinones and nitroaromatics in a single-electron way [19,30,31]. For quinone reduction by NAD(P)H-oxidizing flavoenzymes, the single-electron flux is defined as a ratio of the rate of 1,4-benzoquinone-mediated reduction of the added cytochrome *c* to the doubled rate of 1,4-benzoquinone-mediated NAD(P)H enzymatic oxidation at pH < 7.2 [30]. This approach is based on the fast reduction of cytochrome *c* by 1,4-benzosemiquinone ($k \sim 10^6 \text{ M}^{-1}\text{s}^{-1}$), and its slow reduction by the hydroquinone form. We found that for enzymatic reduction of 50–100 μM 1,4-benzoquinone by 50–100 μM NADPH, the single-electron flux was equal to $54 \pm 4.0\%$ of the total flux. The assessment of the single-electron flux in the reduction of aromatic nitrocompounds can be based on the ArNO_2^- -mediated reduction of added cytochrome *c*. We found that, in the presence of 50 μM NADPH and 100 μM TNT or *p*-nitrobenzaldehyde, the rate of *Rp*FNR-catalyzed reduction of added 50 μM cytochrome *c* was equal to $91 \pm 2.0\%$ and $97 \pm 3.0\%$ of the doubled NADPH oxidation rate, respectively. These reactions were inhibited by 100 U/mL superoxide dismutase by 49% and 37%, respectively, which reflects the rapid reoxidation of ArNO_2^- with O_2 and the participation of superoxide in the reduction of cytochrome *c*. Thus, one may conclude that *Rp*FNR reduces ArNO_2 in a single-electron way.

Finally, we examined the inhibition of quinone reductase reaction of *Rp*FNR by the reaction product NADP^+ . At a fixed juglone concentration (200 μM), NADP^+ acted as a competitive inhibitor toward NADPH (Figure 5A) with $K_{\text{is}} = 150 \pm 10 \mu\text{M}$, as deduced from Equation (4). In turn, at a fixed concentration of 100 μM NADPH, NADP^+ acts as an apparently noncompetitive inhibitor toward juglone (Figure 5B) with $K_{\text{ii}} = 1.7 \pm 0.1 \text{ mM}$, as obtained using Equation (5).

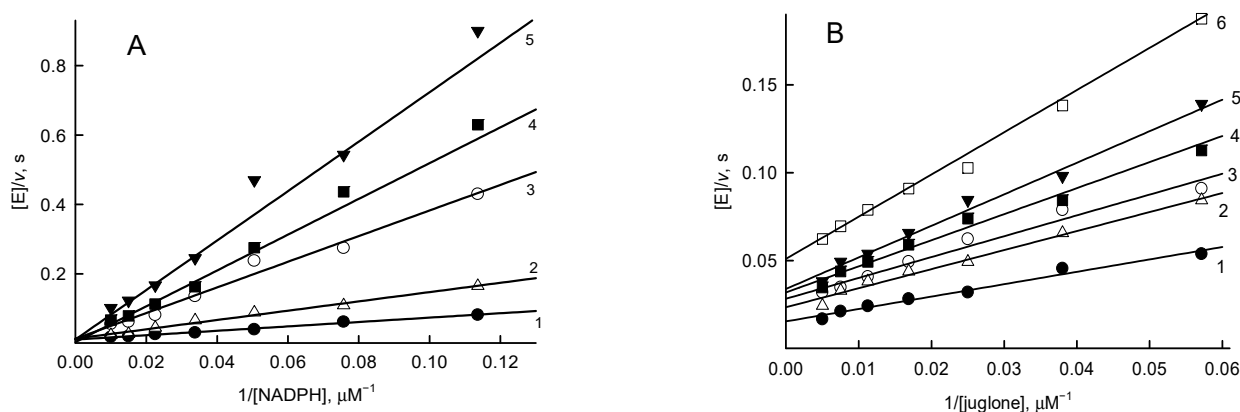


Figure 5. Inhibition of *RpFNR*-catalyzed reactions by NADP⁺. (A) Competitive inhibition of the juglone reductase reaction of *RpFNR* by NADP⁺ at varied concentration of NADPH and in the presence of 200 μM juglone. NADP⁺ concentrations are 0 (1), 0.25 mM (2), 0.5 mM (3), 0.75 mM (4), and 1.0 mM (5). (B) Noncompetitive inhibition at varied juglone concentration in the presence of 100 μM NADPH. NADP⁺ concentrations are 0 (1), 0.5 mM (2), 1.0 mM (3), 1.5 mM (4), 2.0 mM (5), and 3.0 mM (6).

3.3. *RpFNR* Oxidation under Multiple Turnover Conditions

The spectral changes of *RpFNR*-bound FAD during its multiple turnover under aerobic conditions in the presence of NADPH and tetramethyl-1,4-benzoquinone (duroquinone) provides insight into the reoxidation mechanism of the enzyme. Duroquinone does not possess absorbance at ≥ 460 nm; besides, its semiquinone form is rapidly reoxidized by oxygen [28]. Control experiments were performed without the addition of a quinone, and the initial fast phase of FAD reduction by NADPH observed at 460 nm was followed by a slow reoxidation by oxygen (Figure 6A). A transient increase in absorbance at 600 nm at the same time scale accompanies this process (Figure 6A). In the presence of quinone, the reoxidation of FADH⁻ and the disappearance of the 600 nm absorbing species are accelerated by more than one order of magnitude (Figure 6B).

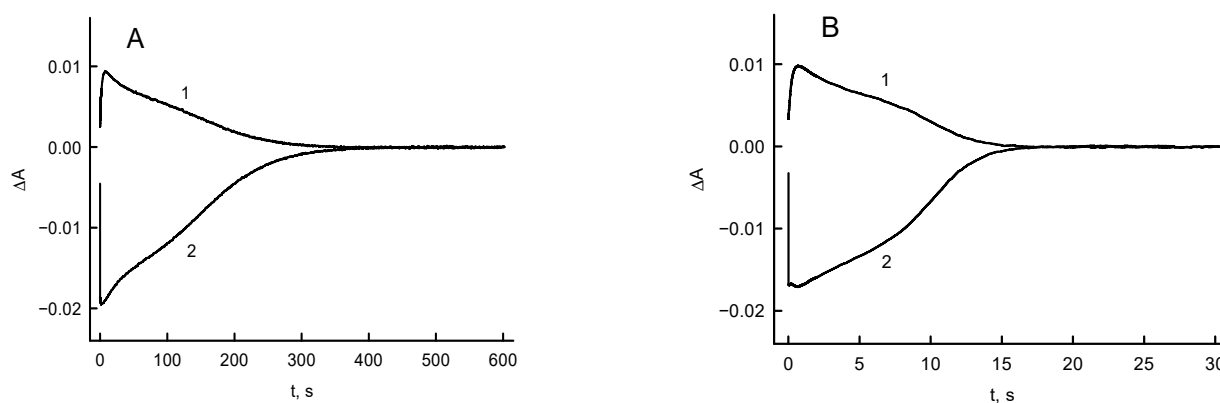


Figure 6. The absorbance changes at 600 nm (1) and 460 nm (2) during the reduction of *RpFNR* (4.0 μM) by 50 μM NADPH and its subsequent reoxidation by oxygen (A) or 250 μM duroquinone (B). Concentrations are reported after mixing.

The maximal ΔA_{460} after the enzyme mixing with NADPH (Figure 6A) corresponds to 90% of *RpFNR* FAD absorbance decrease after the enzyme mixing with an excess NADPH under anaerobic conditions [15,16]. Assuming that the maximal concentration of the reduced enzyme form under aerobic conditions is 90% of total enzyme, for the reoxidation of *RpFNR* with oxygen (Figure 6A), using Equation (6) we obtain a $k_{ox} = 0.11 \pm 0.01$ s⁻¹, which was close to the steady-state NADPH oxidase activity of *RpFNR*. In the presence of

250 μM tetramethyl-1,4-benzoquinone, we obtain a $k_{\text{ox}} = 2.05 \pm 0.07 \text{ s}^{-1}$, which is close to the steady-state reduction rate of this oxidant (Table 1).

In order to characterize the reaction intermediates absorbing at 600 nm (Figure 6), the measurements were performed at different wavelengths. The results show that the absorbance initially increased in the range of 525–750 nm with $\lambda_{\text{max}} \sim 720 \text{ nm}$ (Figure 7). Subsequently, the formation and decay of a secondary flat absorbance band with a maximum at 600–700 nm took place (Figure 7). One may note that the formation of the transient species is not caused by the interaction of isoalloxazine ring of FAD and quinone, because the analogous transient absorbance spectra were obtained during the reoxidation of *RpFNR* with oxygen (data not shown).

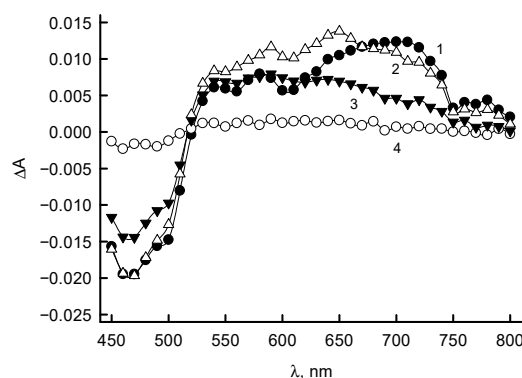


Figure 7. Spectra of reaction intermediates formed during the turnover of *RpFNR*. Difference in absorbance is shown at several timepoints over the 450–800 nm wavelength range. Concentrations of *RpFNR*, 4.0 μM ; NADPH, 50 μM ; and duroquinone, 250 μM (after mixing). Spectra correspond to absorbance changes at 100 ms (1), 1 s (2), 5 s (3), and 20 s (4).

4. Discussion

Due to the large differences in the structure between plant-type and TrxR-type FNRs, the main focus of this work was to disclose the possible differences and similarities in their redox properties. In addition to the mechanistic aspects of studies of the reactions of *RpFNR* with redox active xenobiotics, an important aspect is that *R. palustris* is a model microorganism of anaerobic metabolism of organic compounds [18] in which *RpFNR* may be involved.

In this work, the redox potentials of a representative of TrxR-type FNR were identified for the first time. The E^0_7 of *RpFNR*, -0.276 V (Figure 2A), is close to the redox potential of plant-type FNR from *P. falciparum*, -0.280 V [32], and less negative than that of spinach FNR, -0.342 V [8]. It is currently difficult to draw conclusions about the reasons for these differences. However, we can mention some factors that may lead to a relatively high $\text{FADH}\cdot$ stability, 26.5% at equilibrium, which is comparable to that of semiquinone of spinach FNR, 27% at pH 7.0 [8], and *Anabaena* FNR, 22% at pH 8.0 [33]. *RpFNR* lacks the specific *Anabaena* FNR ion pair Ser80-Glu301 [34] (Ser96-Glu312 in spinach FNR [35]), which forms a H-bond with isoalloxazine N5 and most significantly contributes to $\text{FADH}\cdot$ stability. However, based on structural data of other FNRs and flavodoxins, the stability of $\text{FADH}\cdot$ may be enhanced by the π - π interaction of isoalloxazine with Tyr328 (Tyr98 in *Desulfovibrio vulgaris* flavodoxin [36], Tyr303 in *Anabaena* PCC7119 FNR [37]), formation of H-bonds of isoalloxazine N3 with the carboxy oxygen of Asp56 (Glu59 of *Clostridium beijerinckii* flavodoxin [38]), and O2 with the amide nitrogen of Ile300 (Ile356 of adrenodoxin reductase [39]). The data obtained suggest that the likely direction of electron transfer catalyzed by *RpFNR* is the reduction of Fd at the expense of NADPH.

The “ping-pong” mechanism of quinone reduction by *RpFNR* (Figure 3), pointing to the occurrence of separate reductive and oxidative half-reactions, is common to other FNRs [19,31]. As in our previous studies of *Anabaena* and *P. falciparum* FNR [19,31], no strict oxidant specificity in the reduction of quinones, aromatic nitrocompounds, and *N*-oxides

by *RpFNR* can be discerned from our data except for an increase in their $\log k_{\text{cat}}/K_m$ with E^{1_7} (Figure 4). This suggests a possible applicability of the “outer sphere” electron transfer model [40]. According to this model, the bimolecular rate constant of the electron transfer between the reactants (k_{12}) is expressed as

$$k_{12} = (k_{11} \times k_{22} \times K \times f)^{1/2}, \quad (7)$$

where k_{11} and k_{22} are the electron self-exchange rate constants of the reactants, K is the equilibrium constant of the reaction ($\log K = \Delta E^1 / 0.059 \text{ V}$), and f is expressed as

$$\log f = (\log K)^2 / 4 \log (k_{11} \times k_{22} / Z^2), \quad (8)$$

where Z is the frequency factor, $10^{11} \text{ M}^{-1}\text{s}^{-1}$ [40]. According to Equations (7) and (8), in the reaction of the electron donor with a series of homologous oxidants (which display the same k_{22}), $\log k_{12}$ will exhibit a parabolic (square) dependence on ΔE^1 with a slope 8.45 V^{-1} at $\Delta E^1 = \pm 0.15 \text{ V}$. Because $k_{22} = \sim 10^6 \text{ M}^{-1}\text{s}^{-1}$, characteristic of nitroaromatics, is 100-fold lower than that of quinones and aromatic *N*-oxides, $k_{22} = \sim 10^8 \text{ M}^{-1}\text{s}^{-1}$, the reactivity of ArNO_2 is about 10-fold lower when compared to quinones and $\text{ArN} \rightarrow \text{O}$ of similar E^{1_7} values [41,42]. In this context, it can be noted that the reactivity of *RpFNR* in reactions with both quinones and ArNO_2 , i.e., their k_{cat}/K_m , is close to that previously observed in reactions with plant-type *PfFNR* and *Anabaena* FNR [19,31]. On the other hand, for reasons not yet known, AcPyP^+ is 10 times better at oxidizing *RpFNR* (Figure 2A) than *PfFNR* [19]. Since the k_{cat} of reactions vary considerably (Table 1), it can be suggested that the limiting stage of the catalytic cycle is the oxidative half-reaction. The data of the Figure 5A show that the dominant mechanism of inhibition of the reaction product NADP^+ is its competition with NADPH for binding to the oxidized form of the enzyme. The noncompetitive NADP^+ inhibition with respect to the oxidant (Figure 5B) is slightly different from the uncompetitive inhibition of analogous *Anabaena* and *P. falciparum* FNR-catalyzed reactions [19,31]. This is most likely related to the binding of NADP^+ to the reduced form of the enzyme with low affinity [16].

According to previous studies, photoreduced *Anabaena* FNR was reoxidized by quinones in two steps, $\text{FADH}^- \rightarrow \text{FADH}\cdot$, and $\text{FADH}\cdot \rightarrow \text{FAD}$, with the rate-limiting $\text{FADH}\cdot$ oxidation step [31,43]. This was evidenced by a transient formation of $\text{FADH}\cdot$ with 600 nm absorption. The reoxidation of *RpFNR* should also involve single-electron transfer steps, since it reduces quinones in a predominantly single-electron way. Because the decay of the transient 600 nm absorption and the enzyme reoxidation monitored at 460 nm proceeds with a similar rate (Figure 6B), the FADH oxidation can be a rate-limiting step in quinone reduction by *RpFNR*. However, the absorption characteristics of *RpFNR* multiple turnover intermediates (Figure 7) differ from those of $\text{FADH}\cdot$ formed in the absence of NADP^+ (Figure 2B), although over time they become more similar. Absorption above 700 nm is not characteristic of FADH [24] and indicates the parallel formation of other reaction intermediates. For example, $\text{FADH}^- - \text{NADP}^+$ charge-transfer complexes absorb up to 1000 nm [44]. However, this possibility is ruled out because the spectrum of the intermediates ends at 770–800 nm (Figure 7). In addition, the $\text{FADH}^- - \text{NADP}^+$ complexes possess $\epsilon \sim 1.0 \text{ mM}^{-1}\text{cm}^{-1}$ at 610–725 nm [45]; thus, they would give about three times less increase in absorption than we see in Figure 6. Most likely, the data in Figure 7 reflect the formation of $\text{FADH}\cdot - \text{NADP}(\text{H})$ complexes observed in adrenodoxin reductase, which absorb at $\lambda > 700 \text{ nm}$ but are only partly characterized [46,47].

The catalytic cycle of *RpFNR* should be characterized by significant movement of the FAD- and $\text{NADP}(\text{H})$ -binding domains relative to each other, including the motions of flexible C-terminal region [10,13,16,48]. Hypothetically, this could lead to shielding and deshielding of the FAD isoalloxazine ring, potentially complicating the access of oxidants. The electron exchange rate constants (k_{11}) of metalloproteins can be used to estimate the

electron transfer distance (R_p) during the reactions with inorganic complexes at infinite ionic strength, where the electrostatic interactions are absent [49]

$$R_p (\text{Å}) = 6.3 - 0.35 \ln k_{11}. \quad (9)$$

We applied this approach to the analysis of reactions of FNRs and other single-electron transferring flavoenzymes with uncharged aromatic oxidants, quinones, and nitroaromatics and obtained R_p levels of 5.0 Å (Q) and 4.4 Å (ArNO₂) for *Anabaena* FNR, and 4.8–5.0 Å (Q) and 4.9–5.6 Å (ArNO₂) for *P. falciparum* FNR [19]. However, a systematic overestimation of the electron transfer distances in this case is possible, because the dimethylbenzene part of the FAD isoalloxazine ring of the above enzymes is partly exposed to the solvent [2,5,16]. Therefore, the obtained values may be of limited usefulness only in approximately assessing the “intrinsic” flavoenzyme reactivity. For the reactions of *Rp*FNR with Q and ArNO₂, the approximate k_{11} values may be obtained from the data of Figure 3 at $\Delta E^1_7 = 0$, where $k_{12} = (k_{11} \times k_{22})^{1/2}$. At E^1_7 of the oxidant being equal to -0.285 V, the $\log k_{11}$ values are equal to 1.36 ± 0.46 (quinones) and 1.04 ± 0.22 (nitroaromatics), which then gives $R_p = 5.2 \pm 0.4$ Å and $R_p = 5.4 \pm 0.2$ Å, respectively, according to Equation (9). It can be noted that the possible uncertainty of the E-FADH₂ potential in the range of 10–15 mV has almost no effect on the R_p value, changing it by only 0.1 Å. Thus, these R_p s are close to the R_p values for plant-type FNRs given above, indicating that possible steric interferences in the structure of *Rp*FNR may not affect the low M_r oxidant reduction rate. These data will be valuable in our further studies focusing on the specific features of the interaction of *Rp*FNR with its ferredoxin-type redox partners.

5. Conclusions

Despite structural differences, many of the redox properties of TrxR-type *Rp*FNR redox are similar to those of plant-type FNR: (i) the standard redox potential of FAD and its neutral semiquinone stability, (ii) single-electron reduction of quinones and nitroaromatic compounds, their reactivity and its dependence on single-electron reduction potential, (iii) transient FAD semiquinone formation, and (iv) calculated electron transfer distances. The slight differences in the action of plant-type and *Rp*FNR are manifested through the much faster reduction of AcPyP⁺ by *Rp*FNR and the different mode of its inhibition by the reaction product NADP⁺. These data may be useful in further studies of the specific interaction of *Rp*FNR with its ferredoxin-type redox partners.

Author Contributions: Methodology and investigation, M.L. and D.S.; writing—original draft preparation, review, and editing, M.L., N.Č. and D.S.; funding acquisition, N.Č. and D.S. All authors have read and agreed to the published version of the manuscript.

Funding: This work was supported by the European Social Fund (measure No. 09.33-LMT-K-712, grant No. DOTSUT-34/09.3.3.-LMT-K712-01-0058/LSS-600000-58) (M.L., N.Č.).

Institutional Review Board Statement: Not applicable.

Informed Consent Statement: Not applicable.

Data Availability Statement: Data is contained within the article.

Acknowledgments: We thank Jonas Šarlauskas and Vanda Miškinienė (Institute of Biochemistry, Vilnius) for their generous gift of nitroaromatic compounds and tirapazamine derivatives.

Conflicts of Interest: The authors declare no conflict of interest. The funders had no role in the design of the study; in the collection, analyses, or interpretation of data; in the writing of the manuscript; or in the decision to publish the results.

References

1. Batie, C.J.; Kamin, H. Electron transfer by ferredoxin: NADP⁺ reductase. Rapid-reaction evidence for participation of a ternary complex. *J. Biol. Chem.* **1984**, *259*, 11976–11985. [[CrossRef](#)]
2. Hurley, J.K.; Morales, R.; Martínez-Júlvez, M.; Brodie, T.B.; Medina, M.; Gómez-Moreno, C.; Tollin, G. Structure–function relationships in *Anabaena* ferredoxin/ferredoxin: NADP⁺ reductase electron transfer: Insights from site-directed mutagenesis, transient absorption spectroscopy and X-ray crystallography. *Biochim. Biophys. Acta BBA-Bioenerg.* **2002**, *1554*, 5–21. [[CrossRef](#)]
3. Ceccarelli, E.A.; Arakaki, A.K.; Cortez, N.; Carrillo, N. Functional plasticity and catalytic efficiency in plant and bacterial ferredoxin-NADP(H) reductases. *Biochim. Biophys. Acta BBA-Proteins Proteomics* **2004**, *1698*, 155–165. [[CrossRef](#)] [[PubMed](#)]
4. Medina, M. Structural and mechanistic aspects of flavoproteins: Photosynthetic electron transfer from photosystem I to NADP⁺. *FEBS J.* **2009**, *276*, 3942–3958. [[CrossRef](#)] [[PubMed](#)]
5. Aliverti, A.; Pandini, V.; Pennati, A.; de Rosa, M.; Zanetti, G. Structural and functional diversity of ferredoxin-NADP⁺ reductases. *Arch. Biochem. Biophys.* **2008**, *474*, 283–291. [[CrossRef](#)]
6. Mulo, P.; Medina, M. Interaction and electron transfer between ferredoxin-NADP⁺ oxidoreductase and its partners: Structural, functional, and physiological implications. *Photosynth. Res.* **2017**, *134*, 265–280. [[CrossRef](#)]
7. Monchietti, P.; López Rivero, A.S.; Ceccarelli, E.A.; Catalano-Dupuy, D.L. A new catalytic mechanism of bacterial ferredoxin-NADP⁺ reductases due to a particular NADP⁺ binding mode. *Protein Sci.* **2021**, *30*, 2106–2120. [[CrossRef](#)]
8. Corrado, M.E.; Aliverti, A.; Zanetti, G.; Mayhew, S.G. Analysis of the oxidation-reduction potentials of recombinant ferredoxin-NADP⁺ reductase from spinach chloroplasts. *Eur. J. Biochem.* **1996**, *239*, 662–667. [[CrossRef](#)]
9. Kimata-Arigo, Y.; Yuasa, S.; Saitoh, T.; Fukuyama, H.; Hase, T. Plasmodium-specific basic amino acid residues important for the interaction with ferredoxin on the surface of ferredoxin-NADP⁺ reductase. *J. Biochem.* **2018**, *164*, 231–237. [[CrossRef](#)]
10. Hammerstad, M.; Hersleth, H.-P. Overview of structurally homologous flavoprotein oxidoreductases containing the low M_r thioredoxin reductase-like fold—A functionally diverse group. *Arch. Biochem. Biophys.* **2021**, *702*, 108826. [[CrossRef](#)]
11. Muraki, N.; Seo, D.; Shiba, T.; Sakurai, T.; Kurisu, G. Asymmetric dimeric structure of ferredoxin-NAD(P)⁺ oxidoreductase from the green sulfur bacterium *Chlorobaculum tepidum*: Implications for binding ferredoxin and NADP⁺. *J. Mol. Biol.* **2010**, *401*, 403–414. [[CrossRef](#)] [[PubMed](#)]
12. Seo, D.; Asano, T. C-terminal residues of ferredoxin-NAD(P)⁺ reductase from *Chlorobaculum tepidum* are responsible for reaction dynamics in the hydride transfer and redox equilibria with NADP⁺/NADPH. *Photosynth. Res.* **2018**, *136*, 275–290. [[CrossRef](#)] [[PubMed](#)]
13. Komori, H.; Seo, D.; Sakurai, T.; Higuchi, Y. Crystal structure analysis of *Bacillus subtilis* ferredoxin-NADP⁺ oxidoreductase and the structural basis for its substrate selectivity. *Protein Sci.* **2010**, *19*, 2279–2290. [[CrossRef](#)] [[PubMed](#)]
14. Seo, D.; Soeta, T.; Sakurai, H.; Sétif, P.; Sakurai, T. Pre-steady-state kinetic studies of redox reactions catalysed by *Bacillus subtilis* ferredoxin-NADP⁺ oxidoreductase with NADP⁺/NADPH and ferredoxin. *Biochim. Biophys. Acta BBA-Bioenerg.* **2016**, *1857*, 678–687. [[CrossRef](#)] [[PubMed](#)]
15. Seo, D.; Okabe, S.; Yanase, M.; Kataoka, K.; Sakurai, T. Studies of interaction of homo-dimeric ferredoxin-NAD(P)⁺ oxidoreductases of *Bacillus subtilis* and *Rhodospseudomonas palustris*, that are closely related to thioredoxin reductases in amino acid sequence, with ferredoxins and pyridine nucleotide coenzymes. *Biochim. Biophys. Acta BBA-Proteins Proteomics* **2009**, *1794*, 594–601. [[CrossRef](#)]
16. Seo, D.; Muraki, N.; Kurisu, G. Kinetic and structural insight into a role of the *re*-face Tyr328 residue of the homodimer type ferredoxin-NADP⁺ oxidoreductase from *Rhodospseudomonas palustris* in the reaction with NADP⁺/NADPH. *Biochim. Biophys. Acta BBA-Bioenerg.* **2020**, *1861*, 148140. [[CrossRef](#)]
17. Harwood, C.S.; Gibson, J. Anaerobic and aerobic metabolism of diverse aromatic compounds by the photosynthetic bacterium *Rhodospseudomonas palustris*. *Appl. Environ. Microbiol.* **1988**, *54*, 712–717. [[CrossRef](#)]
18. Ma, Y.; Donohue, T.J.; Noguera, D.R. Kinetic modeling of anaerobic degradation of plant-derived aromatic mixtures by *Rhodospseudomonas palustris*. *Biodegradation* **2021**, *32*, 179–192. [[CrossRef](#)]
19. Lesanavičius, M.; Aliverti, A.; Šarlauskas, J.; Čėnas, N. Reactions of *Plasmodium falciparum* ferredoxin: NADP⁺ oxidoreductase with redox cycling xenobiotics: A mechanistic study. *Int. J. Mol. Sci.* **2020**, *21*, 3234. [[CrossRef](#)]
20. Cichocki, B.A.; Donzel, M.; Heimsch, K.C.; Lesanavičius, M.; Feng, L.; Montagut, E.J.; Becker, K.; Aliverti, A.; Elhabiri, M.; Čėnas, N.; et al. *Plasmodium falciparum* ferredoxin-NADP⁺ reductase-catalyzed redox cycling of plasmodione generates both predicted key drug metabolites: Implication for antimalarial drug development. *ACS Infect. Dis.* **2021**, *7*, 1996–2012. [[CrossRef](#)]
21. Čėnas, N.; Nemeikaitė-Čėnienė, A.; Sergedienė, E.; Nivinskas, H.; Anusevičius, Ž.; Šarlauskas, J. Quantitative structure—Activity relationships in enzymatic single-electron reduction of nitroaromatic explosives: Implications for their cytotoxicity. *Biochim. Biophys. Acta BBA-Gen. Subj.* **2001**, *1528*, 31–38. [[CrossRef](#)]
22. Hay, M.P.; Gamage, S.A.; Kovacs, M.S.; Pruijn, F.B.; Anderson, R.F.; Patterson, A.V.; Wilson, W.R.; Brown, J.M.; Denny, W.A. Structure-activity relationships of 1,2,4-benzotriazine 1,4-dioxides as hypoxia-selective analogues of tirapazamine. *J. Med. Chem.* **2003**, *46*, 169–182. [[CrossRef](#)] [[PubMed](#)]
23. Khan, A.; Ross, W.C. Tumour-growth inhibitory nitrophenylaziridines and related compounds: Structure-activity relationships. *Chem. Biol. Interact.* **1969**, *1*, 27–47. [[CrossRef](#)]
24. Edmondson, D.E.; Tollin, G. Semiquinone formation in flavo- and metalloflavoproteins. *Radic. Biochem.* **1983**, *108*, 109–138. [[CrossRef](#)]

25. Mayhew, S.G. The effects of pH and semiquinone formation on the oxidation-reduction potentials of flavin mononucleotide. A reappraisal. *Eur. J. Biochem.* **1999**, *265*, 698–702. [[CrossRef](#)]
26. Kaplan, N.O.; Ciotti, M.M. Chemistry and properties of the 3-acetylpyridine analogue of diphosphopyridine nucleotide. *J. Biol. Chem.* **1956**, *221*, 823–832. [[CrossRef](#)]
27. Chance, B. A simple relationship for a calculation of the “on” velocity constant in enzyme reactions. *Arch. Biochem. Biophys.* **1957**, *71*, 130–136. [[CrossRef](#)]
28. Wardman, P. Reduction Potentials of One-Electron Couples Involving Free Radicals in Aqueous Solution. *J. Phys. Chem. Ref. Data* **1989**, *18*, 1637–1755. [[CrossRef](#)]
29. Čėnas, N.; Nemeikaitė-Čėnienė, A.; Kosychova, L. Single- and two-electron reduction of nitroaromatic compounds by flavoenzymes: Mechanisms and implications for cytotoxicity. *Int. J. Mol. Sci.* **2021**, *22*, 8534. [[CrossRef](#)]
30. Iyanagi, T.; Yamazaki, I. One-electron-transfer reactions in biochemical systems V. Difference in the mechanism of quinone reduction by the NADH dehydrogenase and the NAD(P)H dehydrogenase (DT-diaphorase). *Biochim. Biophys. Acta BBA-Bioenerg.* **1970**, *216*, 282–294. [[CrossRef](#)]
31. Anusevičius, Ž.; Martínez-Júlvez, M.; Genzor, C.G.; Nivinskas, H.; Gómez-Moreno, C.; Čėnas, N. Electron transfer reactions of *Anabaena* PCC 7119 ferredoxin:NADP⁺ reductase with nonphysiological oxidants. *Biochim. Biophys. Acta BBA-Bioenerg.* **1997**, *1320*, 247–255. [[CrossRef](#)]
32. Balconi, E.; Pennati, A.; Crobu, D.; Pandini, V.; Cerutti, R.; Zanetti, G.; Aliverti, A. The ferredoxin-NADP⁺ reductase/ferredoxin electron transfer system of *Plasmodium falciparum*. *FEBS J.* **2009**, *276*, 3825–3836. [[CrossRef](#)] [[PubMed](#)]
33. Faro, M.; Gómez-Moreno, C.; Stankovich, M.; Medina, M. Role of critical charged residues in reduction potential modulation of ferredoxin-NADP⁺ reductase. *Eur. J. Biochem.* **2002**, *269*, 2656–2661. [[CrossRef](#)] [[PubMed](#)]
34. Medina, M.; Martínez-Júlvez, M.; Hurley, J.K.; Tollin, G.; Gómez-Moreno, C. Involvement of Glutamic Acid 301 in the Catalytic Mechanism of Ferredoxin-NADP⁺ Reductase from *Anabaena* PCC 7119. *Biochemistry* **1998**, *37*, 2715–2728. [[CrossRef](#)] [[PubMed](#)]
35. Aliverti, A.; Deng, Z.; Ravasi, D.; Piubelli, L.; Karplus, P.A.; Zanetti, G. Probing the function of the invariant glutamyl residue 312 in spinach ferredoxin-NADP⁺ reductase. *J. Biol. Chem.* **1998**, *273*, 34008–34015. [[CrossRef](#)]
36. Swenson, R.P.; Krey, G.D. Site-directed mutagenesis of tyrosine-98 in the flavodoxin from *Desulfovibrio vulgaris* (Hildenborough): Regulation of oxidation-reduction properties of the bound FMN cofactor by aromatic, solvent, and electrostatic interactions. *Biochemistry* **1994**, *33*, 8505–8514. [[CrossRef](#)]
37. Nogués, I.; Tejero, J.; Hurley, J.K.; Paladini, D.; Frago, S.; Tollin, G.; Mayhew, S.G.; Gómez-Moreno, C.; Ceccarelli, E.A.; Carrillo, N.; et al. Role of the C-terminal tyrosine of ferredoxin-nicotinamide adenine dinucleotide phosphate reductase in the electron transfer processes with its protein partners ferredoxin and flavodoxin. *Biochemistry* **2004**, *43*, 6127–6137. [[CrossRef](#)]
38. Bradley, L.H.; Swenson, R.P. Role of hydrogen bonding interactions to N(3)H of the flavin mononucleotide cofactor in the modulation of the redox potentials of the *Clostridium beijerinckii* flavodoxin. *Biochemistry* **2001**, *40*, 8686–8695. [[CrossRef](#)]
39. Ziegler, G.A.; Vonrhein, C.; Hanukoglu, I.; Schulz, G.E. The structure of adrenodoxin reductase of mitochondrial P450 systems: Electron transfer for steroid biosynthesis. *J. Mol. Biol.* **1999**, *289*, 981–990. [[CrossRef](#)]
40. Marcus, R.A.; Sutin, N. Electron transfers in chemistry and biology. *Biochim. Biophys. Acta BBA-Rev. Bioenerg.* **1985**, *811*, 265–322. [[CrossRef](#)]
41. Wardman, P.; Dennis, M.F.; Everett, S.A.; Patel, K.B.; Stratford, M.R.L.; Tracy, M. Radicals from one-electron reduction of nitro compounds, aromatic *N*-oxides and quinones: The kinetic basis for hypoxia-selective, bioreductive drugs. *Biochem. Soc. Symp.* **1995**, *61*, 171–194. [[CrossRef](#)] [[PubMed](#)]
42. Nemeikaitė-Čėnienė, A.; Šarlauskas, J.; Jonušienė, V.; Marozienė, A.; Misevičienė, L.; Yantsevich, A.V.; Čėnas, N. Kinetics of flavoenzyme-catalyzed reduction of tirapazamine derivatives: Implications for their prooxidant cytotoxicity. *Int. J. Mol. Sci.* **2019**, *20*, 4602. [[CrossRef](#)] [[PubMed](#)]
43. Anusevičius, Ž.; Misevičienė, L.; Medina, M.; Martínez-Júlvez, M.; Gomez-Moreno, C.; Čėnas, N. FAD semiquinone stability regulates single- and two-electron reduction of quinones by *Anabaena* PCC7119 ferredoxin:NADP⁺ reductase and its Glu301Ala mutant. *Arch. Biochem. Biophys.* **2005**, *437*, 144–150. [[CrossRef](#)]
44. Sánchez-Azqueta, A.; Musumeci, M.A.; Martínez-Júlvez, M.; Ceccarelli, E.A.; Medina, M. Structural backgrounds for the formation of a catalytically competent complex with NADP(H) during hydride transfer in ferredoxin-NADP⁺ reductases. *Biochim. Biophys. Acta BBA-Bioenerg.* **2012**, *1817*, 1063–1071. [[CrossRef](#)] [[PubMed](#)]
45. Tejero, J.; Peregrina, J.R.; Martínez-Júlvez, M.; Gutiérrez, A.; Gómez-Moreno, C.; Scrutton, N.S.; Medina, M. Catalytic mechanism of hydride transfer between NADP⁺/H and ferredoxin-NADP⁺ reductase from *Anabaena* PCC 7119. *Arch. Biochem. Biophys.* **2007**, *459*, 79–90. [[CrossRef](#)] [[PubMed](#)]
46. Kitagawa, T.; Sakamoto, H.; Sugiyama, T.; Yamano, T. Formation of the semiquinone form in the anaerobic reduction of adrenodoxin reductase by NADPH. Resonance Raman, EPR, and optical spectroscopic evidence. *J. Biol. Chem.* **1982**, *257*, 12075–12080. [[CrossRef](#)]
47. Sakamoto, H.; Ohta, M.; Miura, R.; Sugiyama, T.; Yamano, T.; Miyake, Y. Studies on the reaction mechanism of NADPH-adrenodoxin reductase with NADPH. *J. Biochem.* **1982**, *92*, 1941–1950. [[CrossRef](#)]

-
48. Seo, D.; Asano, T.; Komori, H.; Sakurai, T. Role of the C-terminal extension stacked on the re-face of the isoalloxazine ring moiety of the flavin adenine dinucleotide prosthetic group in ferredoxin-NADP⁺ oxidoreductase from *Bacillus subtilis*. *Plant Physiol. Biochem.* **2014**, *81*, 143–148. [[CrossRef](#)]
 49. Mauk, A.G.; Scott, R.A.; Gray, H.B. Distances of electron transfer to and from metalloprotein redox sites in reactions with inorganic complexes. *J. Am. Chem. Soc.* **1980**, *102*, 4360–4363. [[CrossRef](#)]